Mineralogical Magazine, April 2017, Vol. 81(2), pp. 305–317

As-bearing new mineral species from Valletta mine, Maira Valley, Piedmont, Italy: III. Canosioite, $Ba_2Fe^{3+}(AsO_4)_2(OH)$, description and crystal structure

F. Cámara[1,2], E. Bittarello[1,2], M. E. Ciriotti[3], F. Nestola[4], F. Radica[5], F. Massimi[6], C. Balestra[7] and R. Bracco[8]

[1] Dipartimento di Scienze della Terra, Università degli Studi di Torino, via Tommaso Valperga Caluso 35, I-10125 Torino, Italy
[2] CrisDi, Interdepartmental Centre for the Research and Development of Crystallography, via Pietro Giuria 5, I-10125 Torino, Italy
[3] Associazione Micromineralogica Italiana, via San Pietro 55, I-10073 Devesi-Cirié, Torino, Italy
[4] Dipartimento di Geoscienze, Università degli Studi di Padova, via G. Gradenigo 6, I-35131 Padova, Italy
[5] Dipartimento di Scienze Geologiche, Università degli Studi Roma Tre, largo San Leonardo Murialdo 1, I-00146 Roma, Italy
[6] Dipartimento di Ingegneria Meccanica e Industriale, Università degli Studi Roma Tre, via della Vasca Navale 79, I-00146 Roma, Italy
[7] Associazione Micromineralogica Italiana, via Luigi Delfino 74, I-17017 Millesimo, Savona, Italy
[8] Associazione Micromineralogica Italiana, via Montenotte 18/6, I-17100 Savona, Italy

[*Received 16 August 2015; Accepted 3 March 2016; Associate Editor: Stuart Mills*]

ABSTRACT

The new mineral species canosioite, ideally $Ba_2Fe^{3+}(AsO_4)_2(OH)$, has been discovered in the dump of Valletta mine, Maira Valley, Cuneo Province, Piedmont, Italy. Its origin is probably related to the reaction between ore minerals and hydrothermal fluids. It occurs in reddish-brown granules, subhedral millimetre-size crystals, with a pale yellow streak and vitreous lustre. Canosioite is associated with aegirine, baryte, calcite, hematite, bronze Mn-bearing muscovite, unidentified Mn oxides and unidentified arsenates. Canosioite is biaxial (+) with a $2V_{meas} = 84(2)°$. It is weakly pleochroic with X = brownish yellow, Y = brown, Z = reddish brown, $Z > Y > X$. Canosioite is monoclinic, $P2_1/m$, with $a = 7.8642(4)$, $b = 6.1083(3)$, $c = 9.1670(5)$ Å, $\beta = 112.874(6)°$, $V = 405.73(4)$ Å^3 and $Z = 2$. Calculated density is 4.943 g cm^{-3}. The seven strongest diffraction lines of the observed powder X-ray diffraction pattern are [d in Å, (I) (hkl)]: 3.713 (18)(111), 3.304 (100)(21$\bar{1}$), 3.058 (31)(020), 3.047 (59)(10$\bar{3}$), 2.801 (73)(112), 2.337 (24)(220), 2.158 (24)(12$\bar{3}$). Electron microprobe analyses gave (wt.%): Na_2O 0.06, MgO 0.43, CaO 0.02, NiO 0.02, CuO 0.03, SrO 0.42, BaO 49.36, PbO 1.69, Al_2O_3 1.25, Mn_2O_3 3.89, Fe_2O_3 6.95, Sb_2O_3 0.01, SiO_2 0.03, P_2O_5 0.02, V_2O_5 10.88, As_2O_5 24.64, SO_3 0.01, F 0.02, H_2O 1.61 was calculated on the basis of 1 (OH,F,H_2O) group per formula unit. Infrared spectroscopy confirmed the presence of OH. The empirical formula calculated on the basis of 9 O apfu, is $(Ba_{1.92}Pb_{0.05}Sr_{0.02}Na_{0.01})_{\Sigma 2.00}(Fe^{3+}_{0.52}Mn^{3+}_{0.29}Al_{0.15}Mg_{0.06})_{\Sigma 1.02}[(As_{0.64}V_{0.36})_{\Sigma 1.00}O_4]_2[(OH_{0.92}F_{0.01})(H_2O)_{0.07}]$ and the ideal formula is $Ba_2Fe^{3+}(AsO_4)_2(OH)$. The crystal structure was solved by direct methods and found to be isostructural to that of arsenbrackebuschite. The structure model was refined ($R_1 = 2.6\%$) on the basis of 1245 observed reflections. Canosioite is named after the small municipality of Canosio, where the type locality, the Valletta mine, is situated. The new mineral and name were approved by the International Mineralogical Association Commission on New Minerals and Mineral Names (IMA2015-030).

*E-mail: fernando.camaraartigas@unito.it
https://doi.org/10.1180/minmag.2016.080.097

Keywords: canosioite, arsenate, arsenbrackebuschite group, new mineral species, crystal structure, Valletta, Piedmont, Italy.

© 2017 The Mineralogical Society

Introduction

This is the third of a series of new mineral descriptions of As-bearing minerals from the Valletta mine (Cámara *et al*. 2014, 2015*a*). The sample containing canosioite was collected by one of the authors (CB) in the dumps of Valletta mine, Vallone della Valletta, Canosio municipality, Maira Valley, Cuneo Province, Piedmont, Italy (44° 23′54" N, 7°5′37" E, 2560 m asl). Canosioite is named after the small municipality of Canosio, of ~80 inhabitants, where the type locality, the Valletta mine, is situated. The new mineral and name were approved by the International Mineralogical Association Commission on New Minerals, Nomenclature and Classification (|IMA2015-030, Cámara *et al*., 2015*b*). The holotype material is deposited in the mineralogical collection of the Museo Regionale di Scienze Naturali di Torino, Sezione di Mineralogia, Petrografia e Geologia, via Giovanni Giolitti 36, I–10123 Torino, Italy, catalogue number M/15941.

Fig. 1. Reddish-brown granules or subhedral crystals of canosioite on calcite (Field of view = 5 mm) (collection and photo R. Bracco).

Geological setting and mineral occurrence

Historical and geological information on the Valletta mine are summarized in Cámara *et al*. (2014). The deposit at Valletta mine has never been studied from a genetic point of view and available geological data for the area are of limited detail. Moreover, the volume of mineralized body is rather limited on the surface. The mine dumps are the only remains of the former mining activities and consist of dispersed quartzites with quartz veins that contain a large variety of mineral phases rich in arsenic, vanadium, barium and strontium.

The new mineral is associated strictly with minerals such as almost colourless to brownish aegirine, baryte, calcite, hematite, bronze Mn-bearing muscovite, unidentified Mn oxides and unidentified Mn arsenates. Other minerals in specimens from the same dump locality are adelite, albite, arseniopleite, azurite, bariopharmacosiderite, berzeliite, braccoite (IMA 2013-093), braunite, coralloite, cryptomelane, diopside, fianelite, fluorapatite, gamagarite, ganophyllite, grandaite (IMA 2013-059), gypsum, hollandite, ilmenite, magnesio-arfvedsonite, magnesio-riebeckite, magnetite, malachite, manganberzeliite, mimetite, neotocite, opal, orthoclase, palenzonaite, phlogopite, pyrobelonite, quartz, ranciéite, richterite, rhodochrosite, rhodonite, rutile, saneroite, talc, tetrahedrite, tilasite, tiragalloite, titanite, tokyoite, wallkilldellite, As-bearing fianelite, an Fe^{3+}/Mn^{3+}-bearing oxydravite, a uric acid dihydrate-like phase, and some potential new species under study.

Mineralogical characterization

Appearance and physical properties

Well-formed crystals of canosioite are very rare because of the almost total absence of discernible geodes. Only two small specimens of glassy opaque reddish-brown subhedral crystals were found, each around 2.5 mm×1 mm×1 mm in size. Thanks to the natural etching caused by weathering, those crystals were spilling out from a 1.5 cm wide white calcite vein (there were no ultraviolet light

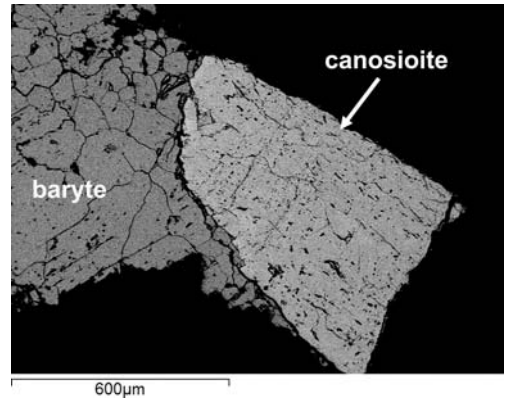

Fig. 2. Back-scattered electron image of a thin section of canosioite (light grey) in association with baryte (medium grey).

responses at 356 and 264 nm). Traces of the same phase are also observed in a fracture of calcite, in the form of micro granules, still of reddish-brown colour, but in this case transparent.

The type sample containing canosioite is small and consists, almost entirely, of calcite and baryte with some strips of hematite and aegirine probably forming a soft and brownish massive material (Figs 1 and 2). Subhedral grained crystals (up to 0.3 mm) form massive aggregates.

Individual crystals are reddish-brown and no twinning was observed. Canosioite is translucent and has a pale yellow streak, a vitreous lustre, and does not fluoresce under shortwave or longwave ultraviolet light. Canosioite is optically biaxial (+) with a $2V_{meas.} = 84(2)°$. The values of refractive index were not determined, but the mean refractive index is estimated as 1.9, i.e. well beyond our available experimental range. Canosioite is weakly pleochroic with X = brownish yellow, Y = brown, Z = reddish brown, $Z > Y > X$.

The mineral is brittle. No cleavage or parting are observed. Hardness was measured by nanoindentation by using an Agilent Nano Indenter G200 at the Università di Roma Tre – LIME labs, performed in CSM (continuous stiffness measurement) mode, with a frequency of 45 Hz, amplitude of oscillation 2 nm, constant strain rate of 0.05 s^{-1}, and a maximum penetration depth of 1000 nm. Results of hardness and modulus profiles were obtained after averaging over 25 different tests. The instrument was completely re-calibrated before testing by performing a series of indentations on a certified amorphous silica reference sample. The observed elastic modulus is 117.9 ± 5.4 GPa (displacement 100–200 nm) and hardness is H: 9.11 ± 0.78 GPa (displacement 100–200 nm); Vickers Hardness was calculated from H in order to calculate Mohs hardness, obtaining Mohs hardness of 6–6½. Because the method for obtaining hardness used a continuous variation of the load, it is difficult to provide actual Vickers hardness units. Density was not measured due to the small crystal size. The calculated density obtained from the empirical formula and unit-cell parameters of the single crystal used for the crystal-structure determination is 4.943 g cm^{-3}.

Chemical data

The chemical composition was determined using a Cameca SX-50 electron microprobe (wavelength-dispersive spectroscopy (WDS) mode) at the Department of Geosciences (Università di Padova) on a mount obtained by embedding a fragment extracted from the holotype close to the place where the crystal used for the diffraction study was extracted. Major and minor elements were determined at 20 kV accelerating voltage and 20 nA beam current (beam size 2 μm), with 40 to 20 s counting time on both peak and background. X-ray counts were converted to oxide wt.% using the *PAP* correction program supplied by Cameca (Pouchou and Pichoir, 1984, 1985). The crystal studied in the thin section was found to be homogeneous (Fig. 2). Elements detected by scanning electron microscopy with energy dispersive X-ray spectroscopy were measured with the electron microprobe in WDS mode except potassium which was below detection limits. The H_2O content was calculated on the basis of one (OH,F,H_2O) per formula unit and additional protons (thus forming H_2O groups) to balance the presence of heterovalent cations; Na^+ at A, Mg^{2+} at M sites. The average of four analyses are given in Table 1.

The empirical formula, calculated on the basis of 9 O apfu (atoms per formula unit), is, within rounding errors, $(Ba_{1.92}Pb_{0.05}Sr_{0.02}Na_{0.01})_{\Sigma 2.00}(Fe^{3+}_{0.52}Mn^{3+}_{0.29}Al_{0.15}Mg_{0.06})_{\Sigma 1.02}[(As_{0.64}V_{0.36})_{\Sigma 1.00}O_4]_2[(OH)_{0.92}F_{0.01}(H_2O)_{0.07}]$ and the simplified formula is $(Ba,Pb,Sr,Na)_2(Fe^{3+},Mn^{3+},Al,Mg)[(As,V)O_4]_2[(OH),F,(H_2O)]$. The ideal formula is $Ba_2Fe^{3+}(AsO_4)_2(OH)$, which requires BaO 49.04, Fe_2O_3 12.77, As_2O_5 36.75, H_2O 1.44, total 100 wt.%.

Electron microprobe data of an unnamed Ba-Fe arsenate, found at the Sn-In-rich Mangabeira A-type Granite (Central Brazil), are quoted in Moura *et al.* (2007), but these data can probably be better assigned to bariopharmacosiderite than to the new species.

Canosioite is unreactive and insoluble in 2 M and 10% HCl, and 65% HNO_3.

Micro-Raman spectroscopy and FTIR

The Raman spectrum of canosioite (Fig. 3) was obtained at the Dipartimento di Scienze della Terra (Università di Torino) using a micro/macro Jobin Yvon Mod. LabRam HRVIS, equipped with a motorized *x*-*y* stage and an Olympus microscope. The back-scattered Raman signal was collected with a 50× objective and the Raman spectrum was obtained for a non-oriented crystal. The 632.8 nm line of a He-Ne laser was used as excitation; laser power (20 mW) was controlled by means of a series of density filters. The minimum lateral and depth

TABLE 1. Analytical data for canosioite.

	Wt.%	Range	SD	Probe standard (crystal, line)
Na_2O	0.06	0.00–0.12	0.05	albite Amelia (TAP, *Kα*)
MgO	0.43	0.35–0.56	0.09	synthetic periclase (TAP,*Kα*)
CaO	0.02	0.00–0.03	0.01	diopside (TAP, *Kα*)
NiO	0.02	0.00–0.05	0.02	NiO (LIF, *Kα*)
CuO	0.03	0.00–0.08	0.04	metallic Cu (LIF, *Kα*)
SrO	0.42	0.26–0.77	0.25	celestine (PET, *Lα*)
BaO	49.36	48.86–50.27	0.65	baryte (LIF, *Lα*)
PbO	1.69	1.47–2.02	0.26	Pb (PET, *Mα*)
Al_2O_3	1.25	1.23–1.27	0.02	corundum (TAP, *Kα*)
Mn_2O_3	3.89	3.65–4.19	0.22	$MnTiO_3$ (LIF, *Kα*)
Fe_2O_3	6.95	6.60–7.18	0.25	Fe_2O_3 (LIF, *Kα*)
Sb_2O_3	0.01	0.00–0.04	0.02	Sb_2S_3 (PET, *Lα*)
SiO_2	0.03	0.01–0.06	0.02	diopside (TAP, *Kα*)
P_2O_5	0.02	0.00–0.08	0.04	apatite (TAP, *Kα*)
V_2O_5	10.88	8.80–9.48	0.48	vanadinite (LIF, *Kα*)
As_2O_5	24.64	24.06–25.34	0.46	synthetic AsGa (TAP, *Lα*)
SO_3	0.01	0.00–0.04	0.02	sphalerite (PET, *Kα*)
F	0.02	0.00–0.09	0.05	fluorite (TAP, *Kα*)
H_2O	1.61	1.58–1.68		
O = F	–0.01	0.00–0.04	0.05	
Total	101.34			

SD – standard deviation.

resolution was set to few μm. The system was calibrated using the 520.6 cm^{-1} Raman band of silicon before each experimental session. The spectra were collected with multiple acquisitions (2 to 3) with single counting times ranging between 20 and 30 s. The spectrum was recorded using the *LabSpec 5* program from 100 to 4000 cm^{-1}. Fourier transform infrared (FTIR, Fig. 4) transmission

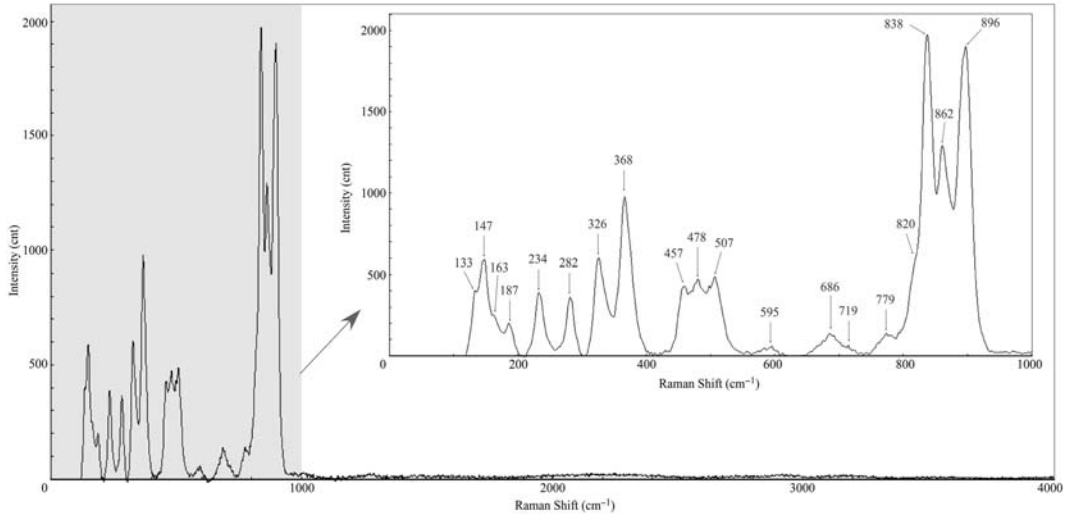

FIG. 3. Raman spectra of canosioite showing the 100–4000 cm^{-1} range and the region between 100 and 1200 cm^{-1} enlarged.

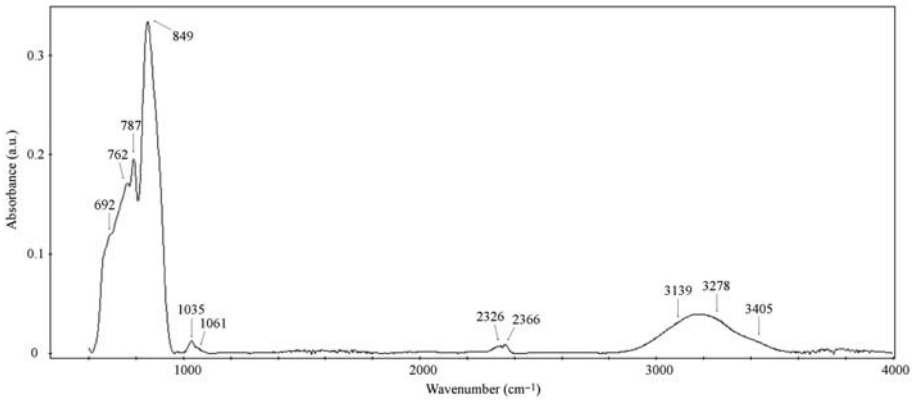

FIG. 4. FTIR spectrum of canosioite in the 100–4000 cm^{-1} region and between 100 and 1200 cm^{-1}.

spectrum (64 scans) recorded using a diamond anvil cell (High Pressure Diamond Optics, Inc.) were obtained with a spectrophotometer Bruker Vertex 70 coupled with a Hyperion 3000 microscope at Centro Conservazione e Restauro "La Venaria Reale" (CCR, Torino Italy) equipped with an MCT detector (Infrared Associates Inc.), working in the spectral range from 4000 to 600 cm^{-1} with an average spectral resolution of 4 cm^{-1}.

The Raman spectrum confirms the presence of $(AsO_4)^{3-}$, although it is very difficult to separate the contributions of arsenate from those of vanadate groups. In the region 200–600 cm^{-1} multiple Raman bands are observed at 234, 282 and 368 cm^{-1} (As^{5+}–O bending vibrations), while bands at 326 cm^{-1} is probably due to V–O bending vibrations (Nakamoto, 1986). Same bands are found in the grandaite ($Sr_2Al(AsO_4)_2(OH)_2$) spectrum (Cámara *et al*., 2014) but are shifted to mostly lower frequencies (213, 308, 347 cm^{-1}). Bands occurring at wavenumbers lower than 200 cm^{-1} correspond to *M*–O and lattice modes (133, 147, 163 and 187 cm^{-1}) according to arsenate vibrations (Myneni *et al*., 1998*a*,*b* and Nakamoto, 1986). Two bands are also observed at those frequencies in grandaite (120 and 162 cm^{-1}). A weak and broad band centred around 480 cm^{-1} is also present, which may be resolved into component bands at 457 and 507 cm^{-1} (As–O) and 478 cm^{-1} (the same for As–O and V–O). Again, that group of bands are also present in grandaite but this time shifted to higher frequencies. In addition grandaite shows bands well resolved at 382 (with shoulder at 386 cm^{-1}), 418 and 425 cm^{-1}. In the region of 600–950 cm^{-1}: weak multiple overlapping bands are observed at 686 and 719 cm^{-1}, not present in grandaite. The three most intense peaks are centred at 838, 862 and 896 cm^{-1} that can correspond to the $(AsO_4)^{3-}$ stretching mode, although they are similar to those expected for the $(VO_4)^{3-}$ groups. A shoulder at 820 cm^{-1} is probably related to the VO_4 symmetric stretching mode (Farmer, 1974). Very similar band frequencies have been observed for grandaite (Cámara *et al*., 2014) which has its three most intense peaks centred at 833, 857 and 899 cm^{-1} (Fig. 5), although the shoulder at 820 cm^{-1} is not present in agreement with its very low V content (Cámara *et al*., 2014). The FTIR spectra are less resolved. However, a large convoluted absorption peak is present at ~850 cm^{-1}, with a weak shoulder at ~790 cm^{-1}. Surprisingly, no bands were observed in the range between 2500 and 4000 cm^{-1} in the Raman spectrum. The absence of strong bands with frequencies higher than 1000 cm^{-1} would indicate the absence of OH groups in canosioite. The same difficulties in observing bands in the range between 2500 and 4000 cm^{-1} of the Raman spectrum were also found in grandaite (Cámara *et al*., 2014). However, the FTIR spectrum in grandaite showed the presence of broad bands centred at ~3150 cm^{-1} and the absence of any discernible clear absorption at ~1650 cm^{-1}, thus confirming the presence of hydrogen as hydroxyl groups but not of (H_2O) as proposed for arsenbrackebuschite (Fig. 4). From the trace amount of F detected in the electron microprobe analysis and, on the basis of crystal structure refinement (see later on), we consider that (OH) groups are also present in canosioite.

X-ray diffraction

The powder X-ray diffraction pattern of canosioite was obtained at CrisDi (Interdepartmental Centre for the Research and Development of Crystallography,

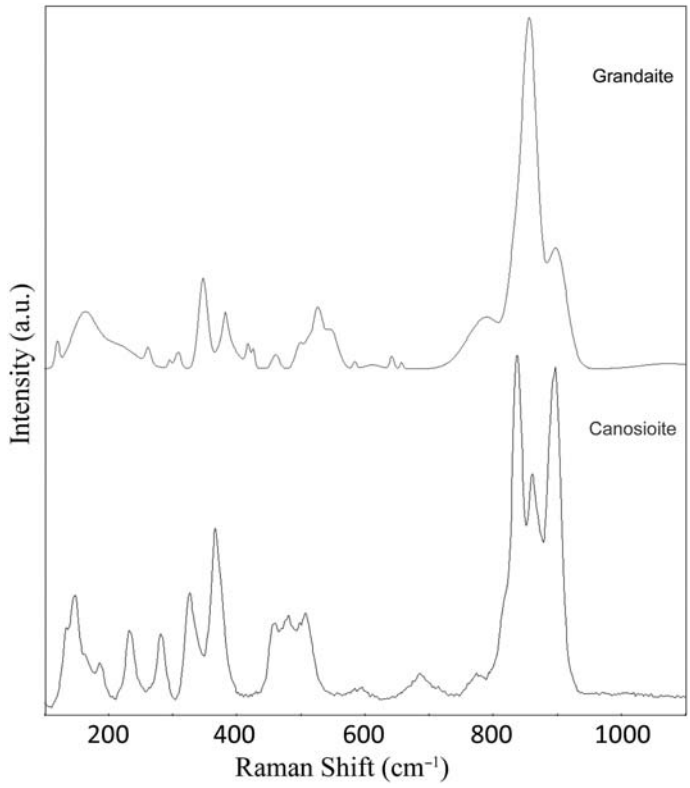

FIG. 5. Raman spectrum of canosioite compared to that of grandaite (Cámara *et al*., 2014) in the 100–1100 cm^{-1} region.

Torino, Italy) using an Oxford Gemini R Ultra diffractometer equipped with a CCD area detector, with graphite-monochromatized Mo*K*α radiation. Indexing of the reflections was based on a calculated powder pattern obtained from the structural model, using the software *LAZY PULVERIX* (Yvon *et al.*, 1977). Experimental and calculated data are reported in Table 2. The unit-cell parameters refined from the powder data with the software *GSAS* (Larson and Von Dreele, 1994) are $a = 7.871(3)$, $b = 6.117(2)$, $c = 9.158(5)$ Å, $\beta = 112.80(3)°$ and $V = 405.9(3)$ $Å^3$.

Single-crystal X–ray diffraction data were collected using an Oxford Gemini R Ultra diffractometer equipped with a CCD area detector at CrisDi (Università di Torino) using graphite-monochromatized Mo*K*α radiation (λ = 0.71073 Å). A crystal fragment of 0.1 mm × 0.05 mm × 0.06 mm, showing sharp optical extinction behaviour was used for collecting intensity data. No crystal twinning was observed. Crystal data and experimental details are reported in Table 3.

The intensities of 2505 reflections with $-11 < h < 9$, $-9 < k < 8$, $-11 < l < 13$ were collected to 64.4°2θ using 1° frame width and an integration time of 5.5 and 22 s (retakes). We collected 3 ω scans, with a total of 207 frames and a detector-to-crystal distance of 55 mm. Data were integrated and corrected for Lorentz and polarization background effects, using the package *CrysAlisPro,* Agilent Technologies, Version 1.171.36.20 (release 27-06-2012 CrysAlis171.36.24). Refinement of the unit-cell parameters was based on 1471 measured reflections. At room temperature, the unit-cell parameters are $a = 7.8642(4)$, $b = 6.1083(3)$, $c = 9.1670(5)$ Å, $\beta = 112.874(6)°$, $V = 405.73(4)$ $Å^3$, space group $P2_1/m$, $Z = 2$. The a:b:c ratio is 1.288:1:1.501. A total of 1405 independent reflections were collected and the structure was solved and refined by means of the *SHELX* set of programs (Sheldrick, 2008). Scattering curves for neutral atoms were taken from International Tables for Crystallography (Wilson, 1992). The structure was refined starting from the atom coordinates of grandaite (Cámara *et al*., 2014). At convergence, a residue in the Fourier difference close to O7 was interpreted as a proton and was added to the model. Hydrogen

TABLE 2. Powder X-ray diffraction data for canosioite.*

h	*k*	*l*	d_{obs}(Å)	d_{calc} (Å)	Int.$_{(obs)}$	Int.$_{(calc)}$
1	1	0	4.674	4.670	7	6
1	**1**	**1**	**3.713**	**3.712**	**18**	**16**
0	1	2	3.470	3.474	9	5
2	**1**	**$\bar{1}$**	**3.304**	**3.304**	**100**	**100**
0	**2**	**0**	**3.058**	**3.054**	**31**	**47**
1	**0**	**$\bar{3}$**	**3.047**	**3.056**	**59**	**69**
2	1	$\bar{2}$	3.037	3.039	13	11
2	0	1	2.941	2.941	11	10
0	2	1	2.874	2.872	15	10
1	2	0	2.817	2.814	9	6
1	**1**	**2**	**2.801**	**2.802**	**73**	**60**
2	1	1	2.651	2.650	8	12
2	1	$\bar{3}$	2.553	2.557	13	9
2	**2**	**0**	**2.337**	**2.335**	**24**	**24**
1	**2**	**$\bar{3}$**	**2.158**	**2.160**	**24**	**36**
3	0	1	2.115	2.115	11	18
3	1	$\bar{4}$	1.921	1.924	18	18
4	0	$\bar{3}$	1.893	1.895	7	8
2	3	$\bar{1}$	1.809	1.808	16	13
1	1	4	1.763	1.765	9	5
3	2	1	1.740	1.739	15	20
1	3	2	1.712	1.711	14	16
4	2	$\bar{2}$	1.652	1.652	13	10
1	2	$\bar{5}$	1.553	1.556	13	9

*Only reflections with $I_{cal} > 6\sigma(I_{cal})$ are listed. The seven strongest reflections are reported in bold.

TABLE 3. Crystal data and summary of parameters describing data collection and refinement for canosioite.

Crystal system	Monoclinic
Space group	$P2_1/m$
Unit-cell dimensions	
a (Å)	7.8642(4)
b (Å)	6.1083(3)
c (Å)	9.1670(5)
β (°)	112.874(6)
V (Å^3)	405.73(4)
Z	2
μ (mm^{-1})	16.71
F(000)	525
D_{calc} (g cm^{-3})	4.943
Crystal size (mm)	0.10 × 0.05 × 0.06
Radiation type	Mo*K*α (0.71073 Å)
Temperature (K)	298
θ range for data collection (°)	4.1–32.2
R_{int}	0.026
Reflections collected	2505
Independent reflections	1405
$F_o>4\sigma(F)$	1245
Refinement method	least-squares matrix: full
No. of refined parameters	88
Final R_{obs} (%) all data	3.3
R_1 (%) $F_o>4\sigma(F)$	2.6
wR_2 (%) $F_o>4\sigma(F)$	5.5
Highest peak/deepest hole (*e* Å^{-3})	1.16/–1.31
Goodness of fit on F^2	1.017

atom coordinates and isotropic displacement parameters were refined without constraints. Refinement converged to $R_1 = 2.58\%$ for 1245 observed reflections with $F_o > 4\sigma(F_o)$ and and 3.30% for all 1405 data and 88 parameters without restraints.

Tables 4, 5 and 6 report displacement parameters, the atomic coordinates, and selected bond distances and angles, respectively, for canosioite. Bond-valence calculations using the parameters of Brown (1981) are reported in Table 7. Tables of structure factors and the crystallographic information file have been deposited with the Principal Editor of *Mineralogical Magazine* and are available from www.minersoc.org/pages/e_journals/dep_mat_mm.html.

Description of the structure

Structure model

The crystal structure of canosioite (Fig. 6) is isostructural with those of members of the brackebuschite supergroup with the general formula of $A_2{}^{VI}M(^{IV}TO_4)_2X$, where $A = Pb^{2+}$, Ba^{2+}, Sr^{2+}, Ca^{2+}, $M = Fe^{3+}$, Al^{3+}, Mn^{3+}, Zn^{2+}, Fe^{2+}, Cu^{2+}, $T = As^{5+}$, V^{5+}, P^{5+}, S^{6+}, $X = OH^-$, F^-, H_2O: chains of $[M^{3+,2+}(T^{5+}O_4)_2X]$ units are connected through interstitial divalent cations (Pb, Sr, Ba for arsenbrackebuschite, grandaite and canosioite, respectively) in the *A* sites [*A*(1) and *A*(2)] (Fig. 5). In canosioite, the interstitial sites *A*(1) and *A*(2) are occupied almost exclusively by Ba and very minor Pb and Sr. The M^{3+} octahedron is occupied dominantly by Fe^{3+} in canosioite, but significant amounts of Mn^{3+} and Al are also present, It shares edges with other *M* octahedra forming a chain along [010]. The shared edge has one anion that, depending on the charge of the cation at the octahedron in each mineral species belonging to the group, can be an OH group or a H_2O molecule, and the other anion is shared with the apex of a $T^{5+}O_4$ tetrahedron [the *T*(1) site]. The remaining four anions coordinating the octahedron are linked to the edge of another $T^{5+}O_4$ tetrahedron

TABLE 4. Atoms, site occupancies, fractional atom coordinates (Å) and equivalent isotropic displacement parameters (Å^2) for the studied canosioite crystal.

Site	Mult.	Occ.	*x/a*	*y/b*	*z/c*	U_{eq}
T(1)	2*e*	0.412(12)As 0.588(12)V	0.43719(9)	¼	0.17014(7)	0.0080(2)
T(2)	2*e*	0.686(14)As 0.314(14)V	0.04486(7)	¼	0.33357(6)	0.00664(19)
M	2*a*	0.233(9)Mg 0.767(9)Fe	0	0	0	0.0078(2)
A(1)	2*e*	0.957(13)Ba 0.043(13)Sr	0.26494(4)	¼	0.75236(4)	0.01679(12)
A(2)	2*e*	0.906(13)Ba	0.67834(4)	¼	0.58533(4)	0.01018(10)
O(1)	4*f*	0.094(13)Sr	−0.0055(4)	0.5185(4)	0.7815(3)	0.0144(6)
O(2)	2*e*		0.2660(5)	¼	0.4567(4)	0.0186(9)
O(3)	2*e*		0.9115(6)	¼	0.4349(5)	0.0245(10)
O(4)	4*f*		0.4942(4)	0.0281(4)	0.2873(3)	0.0173(6)
O(5)	2*e*		0.5514(6)	¼	0.0489(5)	0.0325(12)
O(6)	2*e*		0.1986(5)	¼	0.0466(4)	0.0168(8)
O(7)	2*e*		0.8295(5)	¼	0.9316(4)	0.0123(8)
H(7)	2*e*	1	0.765(14)	¼	0.979(11)	0.07(3)*

*The temperature factor has the form exp(–T) where $T = 8\pi^2 U(\sin(\theta)/\lambda)^2$ for isotropic atomic displacements.

(the *T*(2) site) alternating in both sides. Vanadium is frequently present and is disordered among *T*(1) and *T*(2) sites. It is expected that a complete solid solution exists between canosioite and gamagarite $Ba_2Fe^{3+}(VO_4)_2(OH)$.

The interstitial sites in canosioite are almost fully occupied by Ba, with 0.05 apfu of Pb at *A*(1) and 0.02 apfu of Sr at *A*(2). Vanadium is not dominant at *T* sites and is distributed among both sites but preferentially at *T*(1), which is also slightly larger and more distorted (Table 6). The *T*(1) site is also more distorted in grandaite (Cámara *et al.*, 2014), but not in arsenbrackebuschite, which has a larger and more distorted *T*(2) site (Hofmeister and Tillmanns, 1978), probably due to the distorted coordination of lead at the *A*(1,2) sites.

TABLE 5. Anisotropic displacement parameters* for canosioite (Å).

site	U^{11}	U^{22}	U^{33}	U^{12}	U^{13}	U^{23}
T(1)	0.0077(3)	0.0085(4)	0.0067(3)	0	0.0017(2)	0
T(2)	0.0078(3)	0.0062(3)	0.0062(3)	0	0.0031(2)	0
M	0.0100(4)	0.0067(4)	0.0062(4)	0.0004(3)	0.0025(3)	0.0006(3)
A(1)	0.01548(17)	0.0234(2)	0.01428(18)	0	0.00889(13)	0
A(2)	0.00996(15)	0.01118(16)	0.00970(15)	0	0.00415(11)	0
O(1)	0.0185(13)	0.0121(13)	0.0134(12)	0.0001(11)	0.0071(10)	−0.0009(11)
O(2)	0.0122(17)	0.027(2)	0.0141(18)	0	0.0025(14)	0
O(3)	0.021(2)	0.034(2)	0.028(2)	0	0.0189(18)	0
O(4)	0.0172(13)	0.0136(13)	0.0190(13)	0.0004(11)	0.0047(11)	0.0014(11)
O(5)	0.020(2)	0.063(3)	0.023(2)	0	0.0175(18)	0
O(6)	0.0151(17)	0.0188(19)	0.0151(18)	0	0.0043(14)	0
O(7)	0.0131(17)	0.0098(17)	0.0137(17)	0	0.0047(14)	0

*The temperature factor has the form exp(–*T*) where $T = 2\pi^2\Sigma_{ij}(h(i)h(j)U(i,j)a^*(i)a^*(j))$.

TABLE 6. Main interatomic distances (Å) and geometrical parameters for canosioite.

T(1)–O(4) (×2)	1.679(3)	*A*(1)–O(4) (×2)	2.672(3)
–O(5)	1.679(4)	–O(2)	2.713(4)
–O(6)	1.775(4)	–O(5)	2.775(4)
<*T*(1)–O>	1.703	–O(1) (×2)	2.779(3)
V(Å^3)	2.53	–O(6)	2.939(4)
σ^2*	3.916	–O(3)	3.147(4)
λ*	1.002	<*A*(1)–O>	2.810
		V(Å^3)	33.06
T(2)–O(3)	1.649(4)		
–O(2)	1.665(4)	*A*(2)–O(3)	2.689(4)
–O(1) (×2)	1.719(3)	–O(4) (×2)	2.706(3)
<*T*(2)–O>	1.688	–O(4) (×2)	2.885(3)
V(Å^3)	2.47	–O(7)	2.925(4)
σ^2*	1.485	–O(1) (×2)	2.938(3)
λ*	1.001	–O(2)	2.989(4)
		–O(2) (×2)	3.130(9)
M–O(7) (×2)	1.967(2)	<*A*(2)–O>	2.902
–O(1) (×2)	1.990(3)	*V*(Å^3)	54.60
–O(6) (×2)	2.106(3)		
<*M*–O>	2.021	O(7)–H(7)	0.787(10)
V(Å^3)	10.88	O(7)···O(5)	2.787(6)
σ^2*	24.728	O(5)···H(7)	2.017(10)
λ*	1.009	O(7)–H–O(5)	166(9)°

*Mean quadratic elongation (λ) and the angle variance (σ^2) were computed according to Robinson *et al*. (1971).

Hydrogen bonding

Moderate hydrogen bonding is suggested in the canosioite. An inspection of Table 7 shows that there is one oxygen site with bond valence incidence < 1.5 vu: O(7). There is one short acceptor–donor distance corresponding to a moderate hydrogen bond [O(7)···O(5) = 2.878(10) Å, Table 6]. Using the relation v (cm^{-1}) = 3592 −304×10^9·exp(−d(O···O)/0.1321) (Libowitzky, 1999), we should expect (OH) stretching bands at ~3380 cm^{-1}. Frequencies at ~3150 cm^{-1} are observed in the FTIR spectrum of canosioite (Fig. 4). The positions of one hydrogen atom was observed in the Fourier-difference maps at convergence and was added to the model. In particular, the position observed for the H(7) atom shows a bond with oxygen at the O(7) anion site (0.79(1) Å) with a short H(7)···O(5) distance of 2.017(10) Å. The presence of divalent cations at *M* sites and of monovalent cations at the *A*(1,2) sites must be charge balanced with higher charge at *T*(1,2) sites or can be compensated with some (H_2O) replacing (OH) groups at O(7) as proposed in arsenbrackebuschite (Hofmeister and Tillmanns, 1978). For that reason, 0.07 (H_2O) pfu were calculated (see chemistry section). However, the occupancy of the second proton bonded to the O(7) is far too low to be observed in a Fourier-difference map or to be detected with FTIR with a crushed grain in a diamond anvil cell. It is worth noting that the acceptor oxygen at O(5) site is undersaturated even after calculating the contribution from the hydrogen bond (bond valence incidence of 1.71 vu, Table 7). A similar situation was also observed in grandaite by Cámara *et al.* (2014). In addition, the equivalent displacement parameter for this atom is the highest (*c*. twice all the other anions but O(3)). This reflects a stressed topology that may explain the observed

TABLE 7. Bond-valence calculations for canosioite (Brown, 1981).

Site	*T*(1)	*T*(2)	*M*	*A*(1)	*A*(2)	*H*(7)	Σ
O(1)		1.147$^{\times 2\downarrow}$	0.510$^{x2\downarrow}$	0.259$^{x2\downarrow}$	0.168$^{x2\downarrow}$		2.084
O(2)		1.325		0.310	0.147		1.882
					0.100$^{x2\downarrow}$ $^{x2\rightarrow}$		
O(3)		1.384		0.169	0.330		1.883
O(4)	1.277$^{x2\downarrow}$			0.346$^{x2\downarrow}$	0.315$^{x2\downarrow}$		2.131
					0.194$^{x2\downarrow}$		
O(5)	1.277			0.262		0.176	1.714
O(6)	0.987		0.374$^{x2\downarrow}$ $^{x2\rightarrow}$	0.097			1.832
O(7)			0.543$^{x2\downarrow}$ $^{x2\rightarrow}$		0.174	0.793	2.053
b.v.	4.816	5.002	2.854	2.048	2.205	0.969	17.894/17.794$^{\uparrow}$
Agg. ch.	5.000	5.000	2.941	2.000	2.000	1.000	

Values are expressed in valence units (vu).

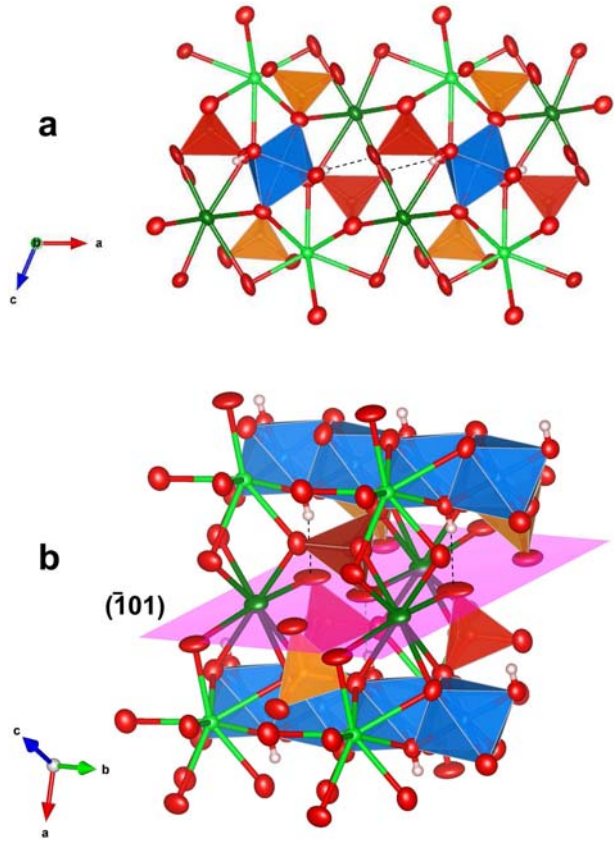

FIG. 6. Detail of the canosioite structure showing: (*a*) the chains of Fe^{3+} octahedral (projected onto [010]), AsO_4 groups and interstitial large cations; (*b*) a detail of the (1̄01) plane perpendicular to the hydrogen bonds. Orange: As tetrahedra (dark *T*(1), light *T*(2)); blue: Fe^{3+} octahedra; green: Ba sites (dark *A*(1), light *A*(2)); white: H sites; red: oxygen sites. O–H···O bond showed with a dashed black line. Thermal displacement ellipsoids shown at 95% probability.

higher distortion at the *T*(1) site. Moreover, the hydrogen bonds are perpendicular to the (1̄01) plane (shown in pink in Fig. 6*b*), which limits the junction of the $[M^{3+,2+}(T^{5+}O_4)_2X]$ units and that includes the *A*(1) sites as well as the O(3) and O(5) anion sites. We hypothesize that this could be a particular weak plane in the structure of these compounds, although no parting has been observed (probably due to the scarcity of material).

Related minerals

Canosioite, $Ba_2Fe^{3+}(AsO_4)_2(OH)$, is the As-dominant analogue of gamagarite, $Ba_2Fe^{3+}(VO_4)_2(OH,H_2O)$ and the Ba-dominant analogue of arsenbrackebuschite, $Pb_2Fe^{3+}(AsO_4)_2(OH,H_2O)$. It is the first Ba member of the arsenbrackebuschite group of the brackebuschite supergroup (Table 8). Group nomenclature follows IMA rules (Mills *et al.*, 2009). Subgroups are divided on the basis of the charge species dominance at the *T* sites. The crystal chemistry of this supergroup is under study as part of a broader project. The observed composition with a significant amount of Mn^{3+} at the *M* site opens the possibility for a possible end-member As-dominant analogue of tokyoite $Ba_2Mn^{3+}(VO_4)_2(OH)$. We have reported a comparison of the properties of the members of the arsenbrackebuschite-group in Cámara *et al.* (2014). In terms of lattice parameters, canosioite is the one showing the largest cell volume among arsenbrackebuschite-group minerals: 405.73(4) Å^3 *vs*. 391.2, 384.2(4) and 366.62(4) Å^3, for arsenbrackebuschite, feinglosite and grandaite, respectively. This is mostly due to the increase of all three lattice parameters. Compared to arsenbrackebuschite, canosioite has larger cell parameters due

TABLE 8. The brackebuschite supergroup (references are given in brackets).

Brackebuschite supergroup, $A1^{2+}\ A2^{2+}\ [^{VI}M_x^{3+}, {}^{VI}M_{1-x}^{2+}]\ [^{IV}(T_x^{5+}, T_{1-x}^{6+})O_4]_2\ (X^-, X)$

Arsenbrackebuschite group dominant at T = As	**Brackebuschite group** dominant at T = V	**Goedkenite group** dominant at T = P	**Tsumebite group** dominant at T = (P or As) + (S or V)
Arsenbrackebuschite[1][2] $Pb_2Fe^{3+}(AsO_4)_2(OH,H_2O)$	Brackebuschite[6][8][9][10][11] $Pb_2Mn^{3+}(VO_4)_2(OH)$	Bearthite[18][19][20] $Ca_2Al(PO_4)_2(OH)$	Arsentsumebite[3][4][5] $Pb_2Cu[(AsO_4)(SO_4)](OH)$
Feinglosite[7] $Pb_2Zn(AsO_4)_2(OH,H_2O)$	Calderónite*[12] $Pb_2Fe^{3+}(VO_4)_2(OH)$	Goedkenite[24] $Sr_2Al(PO_4)_2(OH)$	Bushmakinite[21][22][23] $Pb_2Al[(PO_4)(VO_4)](OH)$
Grandaite[29] $Sr_2Al(AsO_4)_2(OH)$	Gamagarite[13][14][15] $Ba_2Fe^{3+}(VO_4)_2(OH,H_2O)$		Ferribushmakinite[30] $Pb_2Fe^{3+}[(PO_4)(VO_4)](OH)$
Canosioite[31] $Ba_2Fe^{3+}(AsO_4)_2(OH)$	Heyite*[16][30] $Pb_5Fe_2^{2+}(VO_4)_2O_4$		Tsumebite[10][25][25][25][28] $Pb_2Cu[(PO_4)(SO_4)](OH)$
	Tokyoite[17] $Ba_2Mn^{3+}(VO_4)_2(OH)$		

Refs: [1]Abraham *et al*. (1978); [2]Hofmeister and Tillmanns (1978); [3]Vésignié, J.P.L. (1935); [4]Bideaux *et al*. (1966); [5]Zubkova *et al.* (2002); [6]Brackebusch *et al*. (1883); [7]Clark *et al*. (1997); [8]Rammelsberg (1880); [9]Donaldson and Barnes (1955); [10]Fanfani and Zanazzi (1967); [11]Foley *et al*. (1997); [12]González del Tánago *et al*. (2003); [13]de Villiers (1943); [14]Harlow *et al*. (1984); [15]Basso *et al*. (1987); [16]Williams (1973); [17]Matsubara *et al*. (2004); [18]Brunet *et al*. (1993); [19]Brunet and Chopin (1995); [20]Roth (2007); [21]Pekov *et al*. (2002); [22]Yakubovich *et al*. (2002); [23]Pekov (2007); [24]Moore *et al*. (1975); [25]Rosický (1912); [26]Busz (1912); [26]Spencer (1913); [28]Nichols (1966); [29]Cámara *et al*. (2014); [30]Kampf *et al*. (2015); [31]this study; *recent examination on the holotype specimen (BM1972,194) has confirmed the structural correspondence of heyite and calderónite (Kampf *et al*., 2015).

to the substitution of lead by larger barium. In the Strunz System (Strunz and Nickel, 2001) canosioite fits in subdivision 8.B.G, phosphates, etc. with additional anions, without H_2O, with medium-sized and large cations (OH, etc.).

Acknowledgements

The careful review of Peter Leverett and two anonymous reviewer are thanked. Authors wish to thank Bruno Lombardo (CNR-IGG- Torino), Gian Carlo Piccoli, Paolo Bosio and Aldo Marino for their assessment support in field work at Valletta. Marco Nervo (Centro Conservazione e Restauro "La Venaria Reale", Torino Italy) and Tommaso Poli (University of Torino) are thanked for granting access to the FTIR facilities. Raul Carampin (CNR-IGG-Padova, Italy) is thanked for his support on the WDS analysis. FC and EB thank the MIUR and the AMI for the co-funding of a research contract for EB for the year 2013-2014.

References

Abraham, K., Kautz, K., Tillmanns, E. and Walenta, K. (1978) Arsenbrackebuschite, $Pb_2(Fe,Zn)(OH,H_2O)[AsO_4]_2$, a new arsenate mineral. *Neues Jahrbuch für Mineralogie, Monatshefte*, 193–196.

Basso, R., Palenzona, A. and Zefiro, L. (1987) Gamagarite: new occurrence and crystal structure refinement. *Neues Jahrbuch für Mineralogie, Monatshefte*, 295–304.

Bideaux, R.A., Nichols, M.C. and Williams, S.A. (1966) The arsenate analog of tsumebite, a new mineral. *American Mineralogist*, **51**, 258–259.

Brackebusch, L., Rammelsberg, C., Doering, A. and Websky, M. (1883) Sobre los vanadatos naturales de las provincias de Córdoba y San Luis (República Argentina). *Boletín de la Academia Nacional de Ciencias (Córdoba)*, **5**, 439–524.

Brown, I.D. (1981) The bond-valence method: an empirical approach to chemical structure and bonding. Pp. 1–30 in: *Structure and Bonding in Crystals II,* (M. O'Keeffe and A. Navrotsky, editors). Academic Press, New York.

Brunet, F., Gebert, W., Medenbach, O. and Tillmanns, E. (1993) Bearthite, $Ca_2Al[PO_4]_2(OH)$, a new mineral from high-pressure terranes of the western Alps. *Schweizerische Mineralogische und Petrographische Mitteilungen*, **73**, 1–9.

Brunet, F. and Chopin, C. (1995) Bearthite, $Ca_2Al(PO_4)_2OH$: stability, thermodynamic properties and phase relations. *Contributions to Mineralogy and Petrology*, **121**, 258–266.

Busz, K. (1912) Tsumebit, ein neues Mineral von Otavi und Zinnsteinkristalle. *Deutschen Naturforscher und Ärtze in Münster*, **84**, 230–230.

Cámara, F., Ciriotti, M.E., Bittarello, E., Nestola, F., Bellatreccia, F., Massimi, F., Radica, F., Costa, E., Benna, P. and Piccoli, G.C. (2014) Arsenic-bearing new mineral species from Valletta mine, Maira Valley, Piedmont, Italy: I. Grandaite, $Sr_2Al(AsO_4)_2(OH)$, description and crystal structure. *Mineralogical Magazine*, **78**, 757–774.

Cámara, F., Bittarello, E., Ciriotti, M.E., Nestola, F., Radica, F., Marchesini, M. (2015*a*) As-bearing new mineral species from Valletta mine, Maira Valley, Piedmont, Italy: II. Braccoite, $NaMn_5^{2+}[Si_5AsO_{17}(OH)](OH)$, description and crystal structure. *Mineralogical Magazine*, **79**, 171–189.

Cámara, F., Bittarello, E., Ciriotti, M.E., Nestola, F., Radica, F., Massimi, F., Balestra, C. and Bracco, R. (2015*b*) Canosioite, IMA 2015–030. CNMNC Newsletter No. 26, August 2015, page 945; *Mineralogical Magazine*, **79**, 941–947.

Clark, A.M., Criddle, A.J., Roberts, A.C., Bonardi, M. and Moffatt, E.A. (1997) Feinglosite, a new mineral related to brackebuschite, from Tsumeb, Namibia. *Mineralogical Magazine*, **61**, 285–289.

de Villiers, J.E. (1943) Gamagarite, a new vanadium mineral from the Postmasburg manganese deposits. *American Mineralogist*, **28**, 329–335.

Donaldson, D.M. and Barnes, W.H. (1955) The structures of the minerals of the descloizite group and adelite groups: III – brackenbuschite. *American Mineralogist*, **40**, 597–613.

Fanfani, L. and Zanazzi, P.F. (1967) Structural similarities of some secondary lead minerals. *Mineralogical Magazine*, **36**, 522–529.

Farmer V.C. (1974) *The Infrared Spectra of Minerals.* Mineralogical Society, London, 539 pp.

Foley, J.A., Hughes, J.M. and Lange, D. (1997) The atomic arrangement of brackebuschite, redefined as $Pb_2(Mn^{3+},Fe^{3+})(VO_4)_2(OH)$, and comments on Mn^{3+} octahedra. *The Canadian Mineralogist*, **35**, 1027–1033.

González del Tánago, J., La Iglesia, Á., Rius, J. and Fernández Santín, S. (2003) Calderónite, a new lead-iron-vanadate of the brackebuschite group. *American Mineralogist*, **88**, 1703–1708.

Harlow, G.E., Dunn, P.J. and Rossman, G.R. (1984) Gamagarite: a re-examination and comparison with brackebuschite-like minerals. *American Mineralogist*, **69**, 803–806.

Hofmeister, W. and Tillmanns, E. (1978) Strukturelle Untersuchungen an Arsenbrackebuschit. *Tschermaks Mineralogische und Petrographische Mitteilungen*, **25**, 153–163.

Kampf, A.R., Adams, P.M., Nash, B.P. and Marty, J. (2015) Ferribushmakinite, $Pb_2Fe^{3+}(PO_4)(VO_4)(OH)$, the Fe^{3+} analogue of bushmakinite from the Silver Coin mine, Valmy, Nevada. *Mineralogical Magazine*, **79**, 661–669.

Larson, A.C. and Von Dreele, R.B. (1994) *General Structure Analysis System (GSAS).* Los Alamos National Laboratory Report LAUR, 86–748.

Libowitzky, E. (1999) Correlation of OH stretching frequencies and O–H…O hydrogen bond lengths in minerals. *Monatshefte für Chemie*, **130**, 1047–1059.

Matsubara, S., Miyawaki, R., Yokoyama, K., Shimizu, M. and Imai, H. (2004) Tokyoite, $Ba_2Mn^{3+}(VO_4)_2(OH)$, a new mineral from the Shiromaru mine, Okutama, Tokyo, Japan. *Journal of Mineralogical and Petrological Sciences*, **99**, 363–367.

Mills, S.J., Hatert, F., Nickel, E.H. and Ferraris, G. (2009) The standardisation of mineral group hierarchies: application to recent nomenclature proposals. *European Journal of Mineralogy*, **21**, 1073–1080.

Moore, P.B., Irving, A.J. and Kampf, A.R. (1975) Foggite, $CaAl(OH)_2(H_2O)[PO_4]$; goedkinite, $(Sr,Ca)_2Al(OH)[PO_4]_2$; and samuelsonite $(Ca,Ba)Fe_2^{2+}Mn_2^{2+}Ca_{8-}Al_2(OH)_2[PO_4]_{10}$: Three new species from the Palermo No. 1 Pegmatite, North Groton, New Hampshire. *American Mineralogist*, **60**, 957–964.

Moura, M.A., Botelho, N.F., Carvalho de Mendonça, F. (2007) The indium-rich sulfides and rare arsenates of the mineralized Mangabeira A-type granite, Central Brazil. *The Canadian Mineralogist*, **45**, 485–496.

Myneni, S.C.B., Traina, S.J., Waychunas, G.A. and Logan, T.J. (1998*a*) Experimental and theoretical vibrational spectroscopic evaluation of arsenate coordination in aqueous solutions and solids. *Geochimica et Cosmochimica Acta*, **62**, 3285–3300.

Myneni, S.C.B., Traina, S.J., Waychunas, G.A. and Logan, T.J. (1998*b*): Vibrational spectroscopy of functional group chemistry and arsenate coordination in ettringite. *Geochimica et Cosmochimica Acta,* **62,** 3499–3514.

Nakamoto, K. (1986) *Infrared and Raman Spectra of Inorganic and Coordination Compounds.* Wiley, New York, 432 pp.

Nichols, M.C. (1966) The structure of tsumebite. *American Mineralogist*, **51**, 267–267.

Pekov, I.V. (2007) New minerals from former Soviet Union countries, 1998–2006: new minerals approved by the IMA Commission on New Minerals and Mineral Names. *Mineralogical Almanac*, **11**, 9–51.

Pekov, I.V., Kleimenov, D.A., Chukanov, N.V., Yakubovich, O.V., Massa, W., Belakovskiy, D.I. and, Pautov, L.A. (2002) Bushmakinite $Pb_2Al(PO_4)(VO_4)(OH)$, a new mineral of the brackebuschite group from oxidized zone of Berezovskoye gold deposit, the Middle Urals. *Zapiski Vserossijskogo Mineralogicheskogo Obshchestva*, **131**(2), 62–71 [in Russian].

Pouchou, J.L. and Pichoir, F. (1984) A new model for quantitative analysis: Part I. Application to the analysis of homogeneous samples. *La Recherche Aerospatiale*, **3**, 13–38.

Pouchou, J.L. and Pichoir, F. (1985) `PAP′ φ(ρZ) correction procedure for improved quantitative microanalysis. Pp. 104–106 in: *Microbeam Analysis* (J.T. Armstrong, editor). San Francisco Press, San Francisco, USA.

Rammelsberg, C. (1880) Ueber die vanadinerze aus dem Staat Córdoba in Argentinien. *Zeitschrift der Deutschen Geologischen Gesellschaft*, **32**, 708–713.

Robinson, K., Gibbs, G.V. and Ribbe, P.H. (1971) Quadratic elongation: a quantitative measure of distortion in coordination polyhedra. *Science*, **172**, 567–570.

Rosicky, V. (1912) Preslit, ein neues Mineral von Tsumeb in Deutsch-Südwestafrika. *Zeitschrift für Krystallographie und Mineralogie*, **51**, 521–526.

Roth, P. (2007) Bearthite. Pp. 44–45 in: *Minerals First Discovered in Switzerland and Minerals Named After Swiss Individuals.* Kristallografik Verlag, Achberg, Germany, 239 pp.

Sheldrick, G.M. (2008) A short history of SHELX. *Acta Crystallographica*, **A64**, 112–122.

Spencer, L.J. (1913) A (sixth) list of new mineral names. *Mineralogical Magazine*, **16**, 352–378.

Strunz, H. and Nickel, E.H. (2001) *Strunz Mineralogical Tables. Chemical Structural Mineral Classification System. 9th Edition.* E. Schweizerbart, Ed., Stuttgart (Germany), 870 pp.

Vésignié, J.P.L. (1935) Présentation d'échantillons. *Bulletin de la Société Française de Minéralogie*, **58**, 4–5.

Williams, S.A. (1973) Heyite, $Pb_5Fe_2(VO_4)_2O_4$, a new mineral from Nevada. *Mineralogical Magazine*, **39**, 65–68.

Wilson, A.J.C. (editor) (1992) *International Tables for Crystallography. Volume C: Mathematical, Physical and Chemical Tables.* Kluwer Academic Publishers, Dordrecht, The Netherlands.

Yakubovich, O.V., Massa, W. and Pekov, I.V. (2002) Crystal structure of the new mineral bushmakinite, $Pb_2\{(Al,Cu)[PO_4][(V,Cr,P)O_4](OH)\}$. *Doklady Earth Sciences*, **382**, 100–105 [in Russian].

Yvon, K., Jeitschko, W. and Parthé, E. (1977) LAZY PULVERIX, a computer program, for calculating Xray and neutron diffraction powder patterns. *Journal of Applied Crystallography*, **10**, 73–74.

Zubkova, N.V., Pushcharovsky, D.Y., Giester, G., Tillmanns, E., Pekov, I.V. and Kleimenov, D.A. (2002) The crystal structure of arsentsumebite, $Pb_2Cu[(As,S)O_4]_2(OH)$. *Mineralogy and Petrology*, **75**, 79–88.